J Mater Sci: Mater Electron **(2023) 34:2048**

Photo- and cathodo-luminescence properties of (Lu, Gd)$_2$O$_3$: Ce^{3+}, Tb^{3+} phosphors prepared by sol–gel method

Nengli Wang[1,2,*]

[1] *School of Materials Science and Engineering, Changchun University of Science and Technology, Changchun 130022, China*
[2] *Engineering Research Center of Optoelectronic Functional Materials, Ministry of Education, Changchun University of Science and Technology, Changchun 130022, China*

Received: 8 June 2023
Accepted: 17 September 2023
Published online: 28 October 2023

ABSTRACT

(Lu, Gd)$_2$O$_3$: Ce^{3+}, Tb^{3+} phosphors with different Ce^{3+} and Tb^{3+} contents were prepared by sol–gel method using citric acid as a chelating agent. The effects of Ce^{3+}/Tb^{3+} doping concentration on the crystal structure and photo-/cathodo-luminescence properties of the phosphors were investigated. The X-ray diffraction analysis of the samples shows that the synthesized phosphors are well-crystallized and display a pure Lu$_2$O$_3$ phase, indicating the successful formation of (Lu, Gd)$_2$O$_3$ solid solution host. The phosphors show approximately spherical morphology, uniform distribution of particle size and elements. Upon the excitation of ultra-violet light, the photoluminescence spectra of the phosphors with different Ce^{3+} doping concentrations consist of four emission peaks, which correspond to the $^5D_4 \rightarrow {}^7F_J$ ($J = 6$, 5, 4, and 3) transitions of Tb^{3+} ions, respectively. The photoluminescence spectra of the phosphors with different Tb^{3+} doping concentrations consist of five emission peaks, which correspond to the $^5D_3 \rightarrow {}^7F_4$ and $^5D_4 \rightarrow {}^7F_J$ ($J = 6$, 5, 4, and 3) transitions of Tb^{3+} ions, respectively. Upon the excitation of cathode ray, the (Lu, Gd)$_2$O$_3$: Ce^{3+}, Tb^{3+} phosphors exhibit luminescence spectra similar to that of the samples excited by ultra-violet light and a color-tunable luminescence property. In addition, the energy transfer mechanism between Ce^{3+} and Tb^{3+} ion is also discussed.

1 Introduction

Ce^{3+}/Tb^{3+} doped phosphors have been extensively studied in recent years for their potential applications in three-base color white light-emitting diodes (w-LEDs), cathodoluminescence (CL) phosphors for field emission display (FED) applications, high energy laser technology, cathode-ray tubes (CRT), biological imaging, and so on [1–8]. Especially, in CL bio-imaging application of the phosphors, the size of an electron beam spot is on the order of nanometers, so by using suitable imaging probes, CL microscopy enables multicolor biological imaging with nanoscale spatial resolution [8]. Tb^{3+} ion is an important activator with

Address correspondence to E-mail: wangnengli@cust.edu.cn

https://doi.org/10.1007/s10854-023-11353-2

4f → 4f emission peak in the green spectrum region with high color purity centered at 543 nm, corresponding to $^5D_4 \rightarrow {}^7F_5$ transition. However, due to the absolutely forbidden 4f → 4f electric dipole transition, the absorption transition of Tb^{3+} ion is very weak. Ce^{3+} ion possesses a strong broadband excitation in the near-ultraviolet (NUV) band due to the characteristics of optically allowed 4f → 5d transition from the ground state $^2F_{5/2}$ to 5d level. Using Ce^{3+} ion as a sensitizer in Tb^{3+}-doped phosphors, an efficient energy transfer (ET) is possible between Ce^{3+} and Tb^{3+} ions and the photoluminescence intensity of the phosphors can be increased. Therefore, Ce^{3+} and Tb^{3+} co-doped phosphors have been widely investigated as the green-emitting phosphors because of the high luminescent efficiency upon the electron beam or ultraviolet (UV) light excitation [9–12].

Different types of host materials for Ce^{3+}/Tb^{3+} doped phosphors have been studied. For example, fluoride hosts, including Ln^{3+}:CeF_3 (Ln = Nd, Tb) used as bimodal probes for fluorescence and X-ray computed tomography (CT) [13], Sr_2ScF_7: Ce/Tb nanocrystals for lighting, photonic and biological imaging applications [14], β-Na(Gd, Lu)F_4:Ln^{3+} (Ln = Ce, Eu, Tb) nanoparticles for radio-luminescent materials [15]; Borate hosts, for example $Ba_3Y_2B_6O_{15}$:Ce^{3+}/Tb^{3+} [16], $Sr_3Lu_2(BO_3)_4$: Ce^{3+}/Tb^{3+} [17] phosphors for NUV-excited white LEDs, $Dy^{3+}/Ce^{3+}/Tb^{3+}$-activated MgB_4O_7 phosphor for dosimetry application [18]; Aluminosilicate phosphor $CaAl_2Si_2O_8$: Ce/Tb/Yb for applications in Si-based solar cells as an efficient NUV to near-infrared (NIR) converters [19]; Phosphate phosphor $SrMg_2(PO_4)_2$: Ce^{3+}, Tb^{3+} with tunable luminescence for LEDs devices [20]; And gadolinium oxysulfide phosphor Gd_2O_2S: Tb, which is used as an efficient X-ray-to-light converter in many medical imaging modalities [21].

Until now, there have been few reports about the photoluminescence (PL) and CL properties of Ce^{3+}/Tb^{3+} co-doped phosphors using Lu_2O_3–Gd_2O_3 solid solution as host materials. Lutetium oxide (Lu_2O_3) has cubic crystalline structure, and is an attractive sesquioxide host for optical applications, including high-performance scintillation detector and laser gain media. Lu_2O_3 is photo-thermally and photo-chemically stable and has a wide range of optical transparency from visible to NIR regions. The remarkable advantage of Lu_2O_3 is its high density (9.43 g/cm^3) along with high atomic number (Z = 71 for Lu), which gives Lu_2O_3 with high stopping power for ionizing radiation detection [22, 23]. Similar to Lu_2O_3, gadolinium oxide (Gd_2O_3) also possesses high density (7.407 g/cm^3) and high Z-numbers (Z = 64 for Gd) and favorable physical properties, including high melting point, low thermal expansion, and lower phonon energy, and has been widely studied as the host of luminescent lanthanide (Ln^{3+}) ions for optical application. The similar bixbyite cubic crystal structure of Lu_2O_3 and Gd_2O_3 and the close ionic radii of Lu^{3+} and Gd^{3+} ion make Lu_2O_3–Gd_2O_3 solid solution a promising phosphor host material with a wide range of applications. The large band gaps (5.4–5.5 eV) of Lu_2O_3 and Gd_2O_3 allow them to accommodate the energy levels of different luminescent activators, especially rare-earth ions [24–26]. Rétot et al. reported the investigation of the scintillation properties of Lu_2O_3: Eu^{3+} and $(Lu_{0.5}Gd_{0.5})_2O_3$: Eu^{3+} sesquioxide ceramics. They found that compared with Lu_2O_3: Eu^{3+} ceramics, $(Lu_{0.5}Gd_{0.5})_2O_3$: Eu^{3+} presented a faster intrinsic decay time for Eu^{3+} and showed a reduced afterglow over the hundreds of milliseconds time range and a reduced thermally stimulated luminescence (TSL) intensity over the 10–650 K temperature range, which can be applied as a potential new scintillator with improved time response characteristics [23]. Lu et al. demonstrated that Gd_2O_3: Eu phosphor showed stronger photoluminescence intensity compared with Lu_2O_3: Eu phosphor due to the low electronegativity of Gd^{3+}, and Gd^{3+}-doping in Lu_2O_3: Eu can enhance the PL efficiency of the phosphors [27]. Thus, studies of the preparation and luminescent properties of Ce^{3+}/Tb^{3+} co-doped (Lu, Gd)$_2O_3$ phosphors are meaningful for expanding the applications of Ce^{3+}/Tb^{3+} phosphors in the relevant fields. In this work, a series of Ce^{3+}/Tb^{3+} co-doped (Lu, Gd)$_2O_3$ phosphors with were prepared by sol–gel method using citric acid as the chelating agent. The crystal structures and compositional effects of Ce^{3+}/Tb^{3+} doping on the PL and CL properties of the phosphors were studied. The ET mechanism between Ce^{3+} and Tb^{3+} ions in the phosphors is also discussed.

2 Experimental procedures

In this work, two groups of (Lu, Gd)$_2O_3$: Ce^{3+}, Tb^{3+} phosphor samples were prepared according to the following chemical formulas, i.e., $(Lu_{0.8-x}Gd_{0.15}Ce_xTb_{0.05})_2O_3$ (x = 0.1, 0.2, 0.3, 0.4, 0.5 and 0.6 mol%) and $(Lu_{0.847-y}Gd_{0.15}Ce_{0.003}Tb_y)_2O_3$ (y = 7, 8, 9, 10, 11, 12 and 13 mol%). Taking the sample of one chemical composition as an example, the experimental

procedure is as follows: Stoichiometric amounts of Lu_2O_3, Gd_2O_3, CeO_2 and Tb_4O_7 were weighed according to the above chemical formulas and put in a beaker, then the nitric acid (HNO_3) solution (6 mol/L in concentration) was added into the beaker, which was then put on a magnetic stirrer and stirred at 80 °C for 4 h to form the transparent rare-earth (RE) nitrate solution. Citric acid ($C_6H_8O_7$), which acted as a chelating agent with amount of RE_2O_3: citric acid = 1:1.667 in molar ratio was added into the nitrate solution while the solution was stirred continuously until the homogeneous solution was formed. The beaker with the obtained solution was then put in a thermostat water bath and heated at 70 °C for 4 h to form the wet-gel precursor, which was then dried at 160 °C for 2 h to form the dry-gel. The obtained dry-gel was crushed in an agate mortar, and then calcined at 1000 °C for 2 h in reduction atmosphere to obtain the $(Lu, Gd)_2O_3$: Ce^{3+}, Tb^{3+} phosphor sample. The corresponding schematic representation of the experimental procedure is shown in Fig. 1.

Phase identification of the phosphor samples was conducted by X-ray diffraction (XRD) analysis on a Rigaku Ultima IV diffractometer with CuKα radiation source to evaluate the crystalline structure of the samples. The morphology and element distribution of the phosphors were measured with a TESCAN scanning electron microscope (SEM) attached with an Energy-dispersive spectrometer (EDS, Oxford Instruments). PL and photoluminescence excitation (PLE) spectra of the phosphor samples were measured on a Hitachi F-7000 spectrophotometer with a 150 W xenon lamp as the excitation source. CL spectral of the phosphor samples were measured on a Hitachi F-7000 spectrophotometer coupled with an Optic-Zenith electron-beam-ray system as the excitation source. All the characterizations were conducted at room temperature.

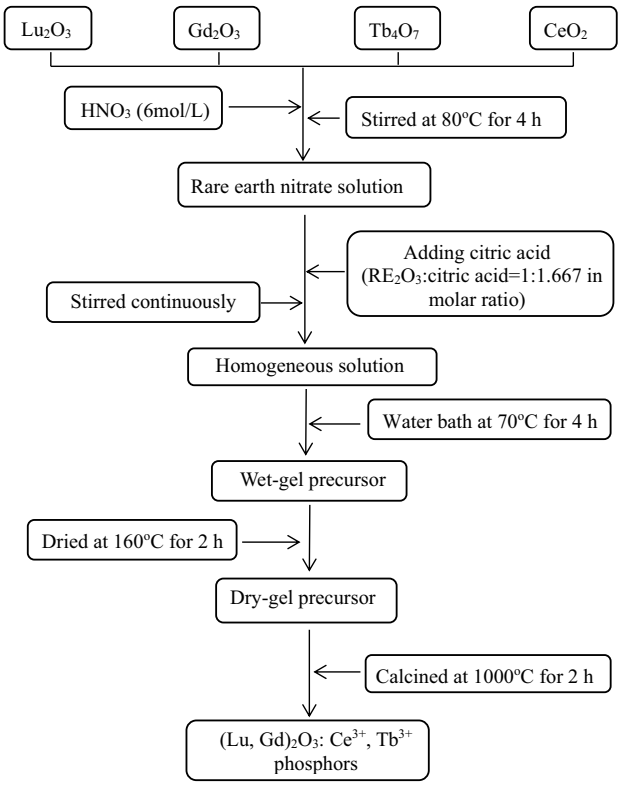

Fig. 1 Schematic representation of the experimental procedure

3 Results and discussion

3.1 XRD patterns and morphology of the (Lu, Gd)$_2O_3$: Ce^{3+}, Tb^{3+} phosphor samples

Figure 2a shows the XRD patterns of the as-prepared $(Lu, Gd)_2O_3$: Ce^{3+}, Tb^{3+} phosphor samples with different Tb^{3+} doping concentrations. The patterns display that all the diffraction peaks of the phosphors are consistent with that of pure Lu_2O_3 phase (JCPDS No. 12-0728), no secondary phases or impurities are detected, indicating that Gd_2O_3 can incorporate well into Lu_2O_3 matrix to form the $(Lu, Gd)_2O_3$ solid solution host. Taking the diffraction peak of (222) crystallographic plane as a reference, it can be seen from the enlarged patterns of Fig. 2b that with the increase of Tb^{3+} doping concentration, the diffraction peaks of the samples shift slightly toward the lower diffraction angle. The ionic radii of the Lu^{3+}, Gd^{3+}, Ce^{3+} and Tb^{3+} ions are 0.848 Å, 0.938 Å, 1.034 Å and 0.923 Å, respectively. Partial substitution of Lu^{3+} ions by Gd^{3+}, Ce^{3+} and Tb^{3+} ions in the Lu_2O_3 matrix can result in the expansion of unit cell and so the increase of interplanar spacing d. According to the Bragg's law $2d\sin\theta = \lambda$, where d is the interplanar spacing, θ is the Bragg angle, λ is the incoming X-ray wavelength, the increase of d results in the decrease of θ. So, with the increase of Tb^{3+} doping concentrations, the diffraction peaks of the samples shift to the lower angles, which further verifies the successful consolidation of Gd^{3+}, Ce^{3+} and Tb^{3+} ions into the Lu_2O_3 matrix. From the XRD analysis results in Fig. 2, the crystallite sizes of the $(Lu, Gd)_2O_3$: Ce^{3+}, Tb^{3+} phosphor samples with different Tb^{3+} doping contents are estimated by the

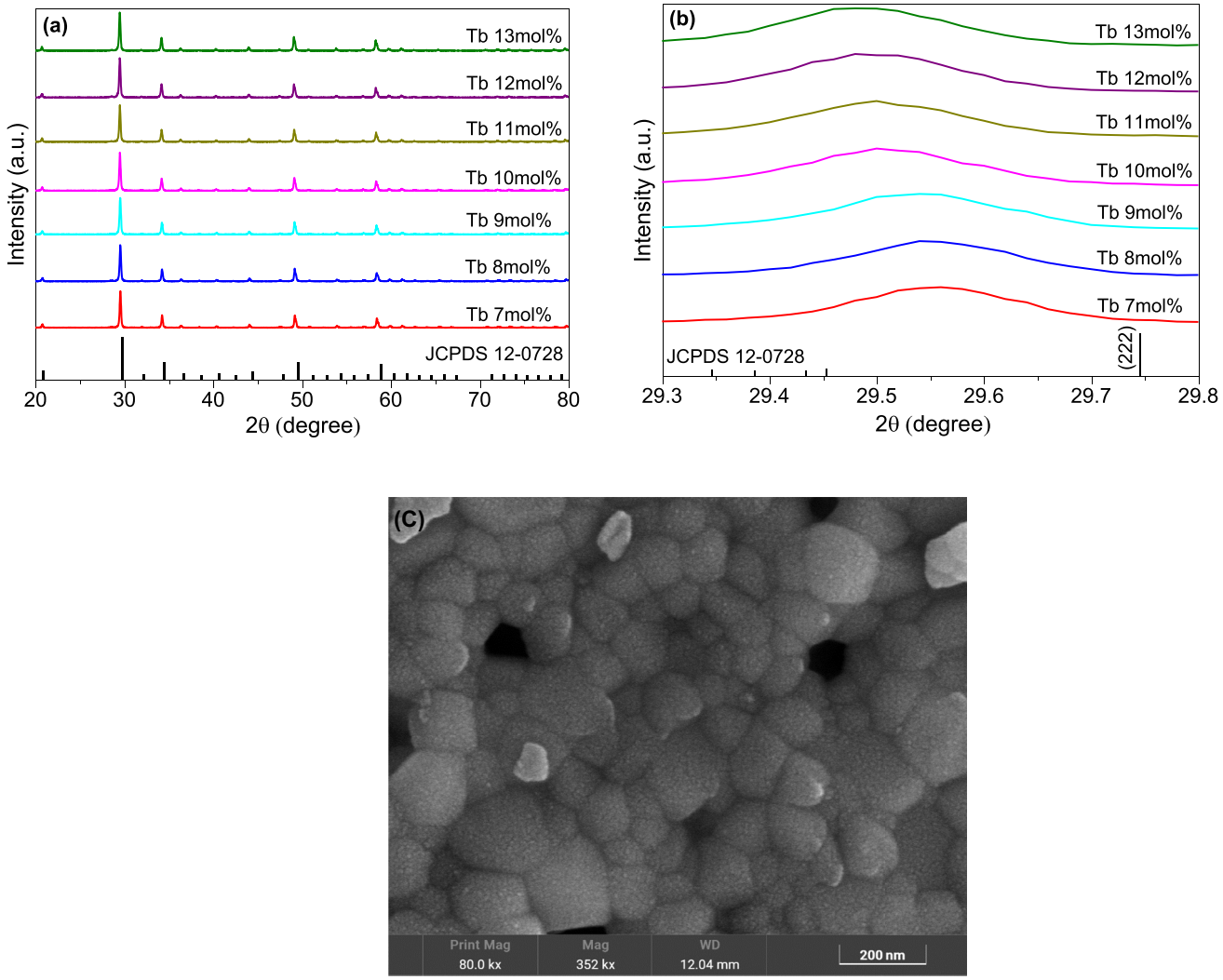

Fig. 2 **a** XRD patterns of the $(Lu, Gd)_2O_3$: Ce^{3+}, Tb^{3+} phosphors with different Tb^{3+} doping concentrations; **b** enlarged XRD pattern between 29.3 and 29.8 degree; **c** SEM image of the phosphor

Scherrer equation, $D = 0.89\lambda/\beta\cos\theta$, where D is the average crystallite size, λ is the x-ray wavelength, θ is the Bragg angle, β is the corrected full-width at half-maximum (FWHM) of the x-ray peak on the 2θ axis [28, 29]. The estimated crystallite sizes of the phosphors with different Tb^{3+} doping contents are between 70 and 82 nm. Figure 2c shows the SEM image of the phosphor sample with 10 mol% Tb^{3+} doping content, the particles of the phosphor show approximately spherical morphology and uniform particle size distribution, and the particle size is at nanoscale. Figure 3 displays the corresponding EDS mapping images of the RE elements in the sample, which indicates the uniform doping of Lu, Gd, Ce and Tb in the sample.

3.2 PL and CL spectral properties of the $(Lu, Gd)_2O_3$: Ce^{3+}, Tb^{3+} phosphors

Figure 4 shows the PLE spectra of the $(Lu_{0.8-x}Gd_{0.15}Ce_xTb_{0.05})_2O_3$ ($x = 0.1$–0.6 mol%) phosphors by monitoring the $^5D_4 \rightarrow {}^7F_5$ emission of Tb^{3+} ($\lambda_{em} = 543$ nm). As shown in Fig. 4, there are strong excitation bands ranging from 240 to 350 nm with the highest intensity centered at 278 nm, which can be attributed to the $4f^1$–$4f^05d^1$ transitions of Ce^{3+} ions. In addition, several very small peaks can be seen in the

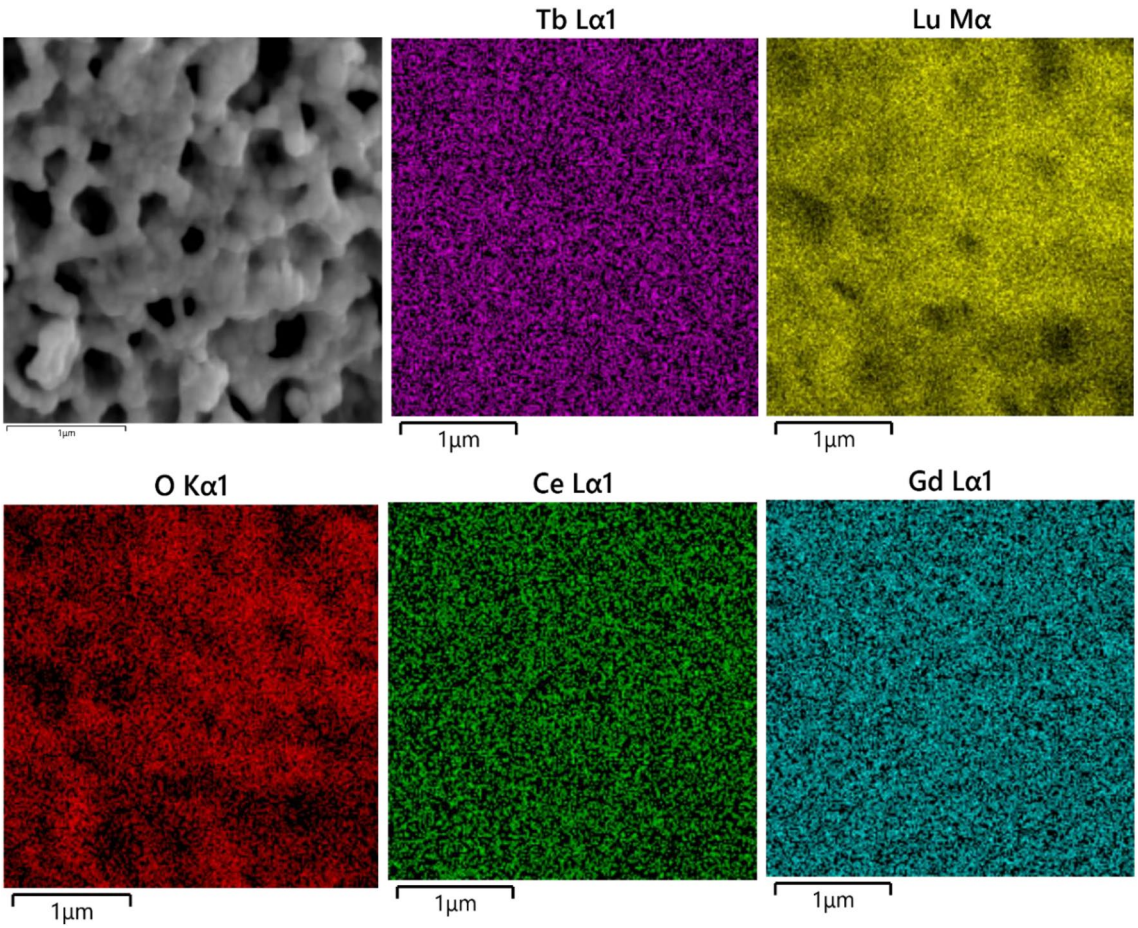

Fig. 3 EDS mapping images of the $(Lu, Gd)_2O_3$: Ce^{3+}, Tb^{3+} phosphors

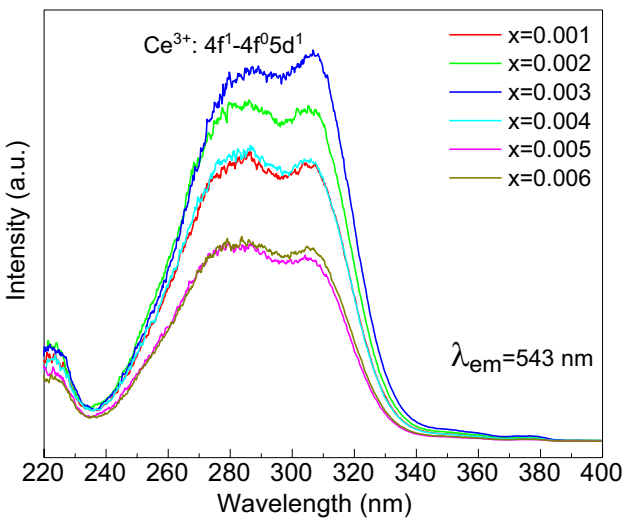

Fig. 4 PLE spectra of the $(Lu_{0.8-x}Gd_{0.15}Ce_xTb_{0.05})_2O_3$ ($x = 0.1$–0.6 mol%) phosphors

range of 350–400 nm, which could be attributed to the f-f transitions of Tb^{3+} ions. Due to the forbidden nature of these transitions, their oscillator strengths are much weaker than that of the spin-allowed $4f^1$–$4f^05d^1$ transitions of Ce^{3+} ions, which reveals that Tb^{3+} ions are essentially excited by Ce^{3+} [30, 31]. The PL spectra of the $(Lu_{0.8-x}Gd_{0.15}Ce_xTb_{0.05})_2O_3$ ($x = 0.1$–0.6 mol%) phosphors ($\lambda_{ex} = 278$ nm) are presented in Fig. 5a. All the samples show obvious PL emission peaks in the range of 450–650 nm, four emission peaks centered at 491, 543, 583 and 623 nm can be assigned to the $^5D_4 \rightarrow {}^7F_J$ ($J = 6$, 5, 4, and 3) transitions of Tb^{3+} ions, respectively [2, 11, 32]. Among the four emission bands, the green light emission at 543 nm, which corresponds to the $^5D_4 \rightarrow {}^7F_5$ transition of Tb^{3+} ions, has the strongest PL emission intensity. The positions and shapes of the PL emission peaks remain constant with the increase of Ce^{3+} ion doping concentration. Taking the PL intensity of 543 nm as a reference, Fig. 5b shows the PL intensities of the $(Lu_{0.8-x}Gd_{0.15}Ce_xTb_{0.05})_2O_3$ ($x = 0.1$–0.6 mol%)

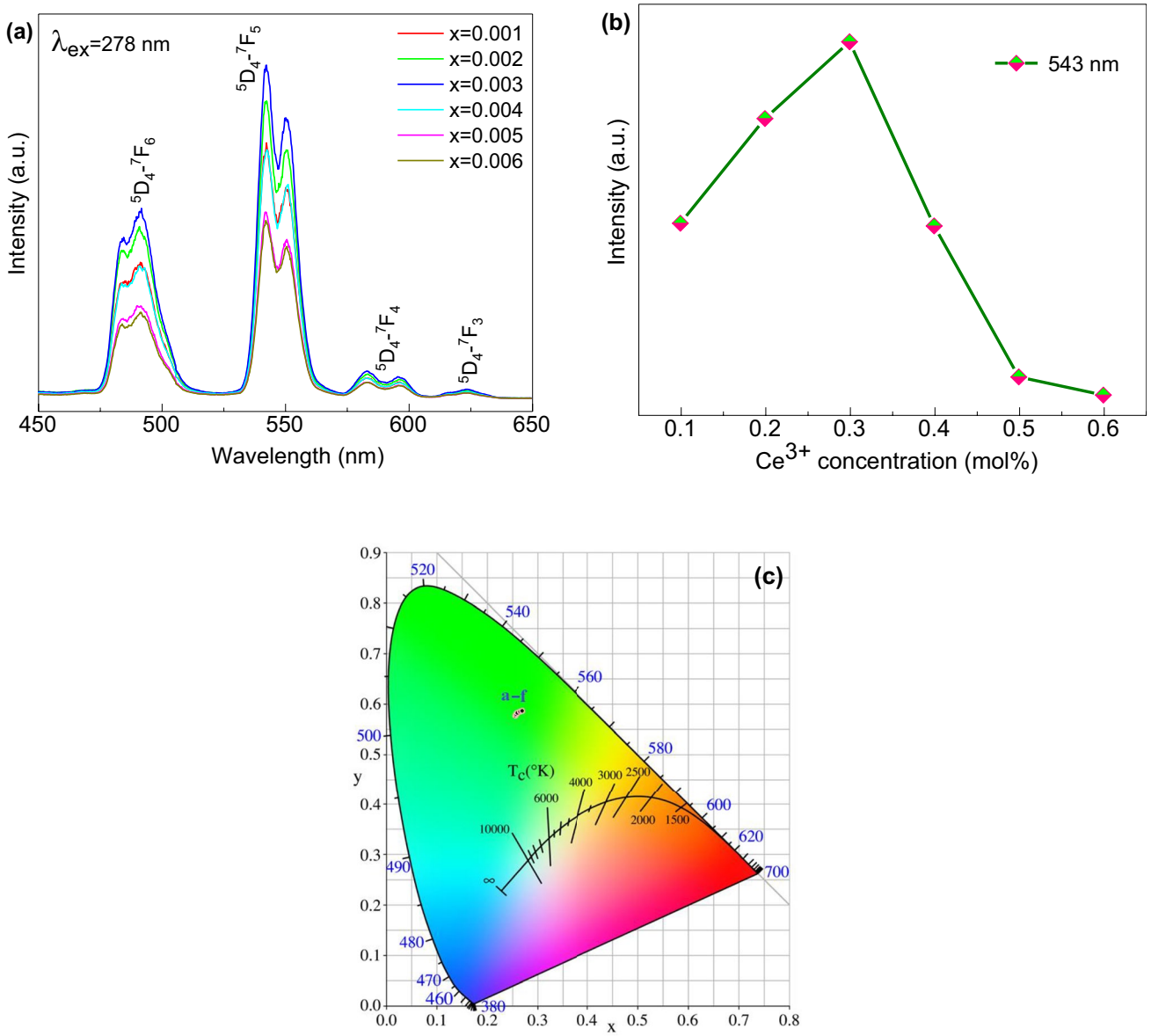

Fig. 5 **a** PL spectra of the $(Lu_{0.8-x}Gd_{0.15}Ce_xTb_{0.05})_2O_3$ ($x = 0.1$–0.6 mol%) phosphors ($\lambda_{ex} = 278$ nm); **b** PL intensity of Tb^{3+} (543 nm) as a function of Ce^{3+} doping concentration; **c** CIE chromaticity coordinate diagram

phosphors at 543 nm as a function of Ce^{3+} doping concentration. The PL intensities of the phosphors increase firstly with the increase of Ce^{3+} concentrations, and reach the maximal value when the Ce^{3+} content is at 0.3 mol%, then decrease with the continuous increase of Ce^{3+} concentration, which may be attributed to the concentration quenching effect. Figure 5c displays the corresponding CIE chromaticity coordinate diagram of the samples. The CIE chromaticity coordinates of 0.1, 0.2, 0.3, 0.4, 0.5 and 0.6 mol% Ce^{3+}-doped phosphors are (0.2587, 0.5819), (0.2554, 0.5776), (0.2573, 0.5801), (0.2595, 0.5826), (0.2657, 0.5848), and (0.2691, 0.5862), respectively. It can be seen that the variation of Ce^{3+} doping content has minor effect on the luminous color of the phosphors, the chromaticity coordinates of the phosphors are close to each other, all in the pure green light region, indicating the color-stability of the phosphors.

Figure 6 shows the PLE spectra of the $(Lu_{0.847-y}Gd_{0.15}Ce_{0.003}Tb_y)_2O_3$ ($y = 7$–13 mol%) phosphors by monitoring the $^5D_4 \rightarrow {}^7F_5$ emission of Tb^{3+} ($\lambda_{em} = 543$ nm). It can be seen from Fig. 6 that by

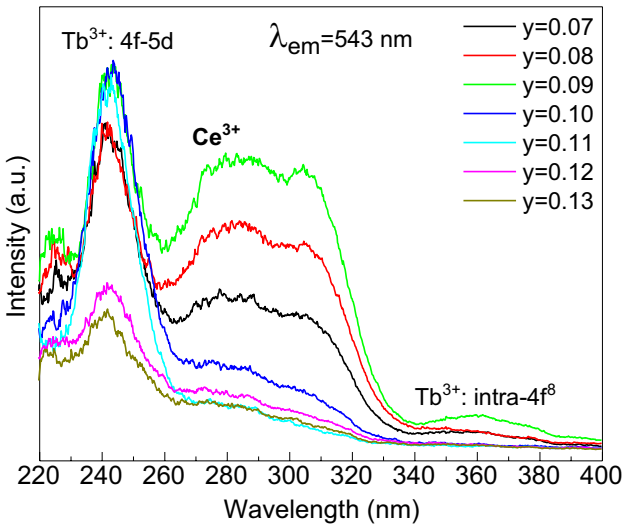

Fig. 6 PLE spectra of the $(Lu_{0.847-y}Gd_{0.15}Ce_{0.003}Tb_y)_2O_3$ ($y = 7$–13 mol%) phosphors

monitoring 543 nm emission of Tb^{3+} ion, the PLE spectra exhibit three excitation bands, the band centered at 243 nm belongs to the 4f-5d transition of Tb^{3+}, the wide band in the range of 260–330 nm can be attributed to the excitation transition of Ce^{3+}, and the weak excitation band in the range of 340–400 nm belongs to the intra $4f^8$ excitation transition of Tb^{3+} [2, 10, 33]. Figure 7a displays the PL spectra of the $(Lu_{0.847-y}Gd_{0.15}Ce_{0.003}Tb_y)_2O_3$ (y = 7–13 mol%) phosphors upon 243 nm excitation. The emission peaks at 468 nm can be assigned to the $^5D_3 \rightarrow {}^7F_4$ transition of Tb^{3+} ion., and the peaks at 491, 543, 583 and 623 nm are due to transitions of $^5D_4 \rightarrow {}^7F_J$ ($J = 6$, 5, 4, and 3) transitions of Tb^{3+} ions, respectively [2, 9, 11, 32, 34]. Among the five emission peaks, the green emission at 543 nm ($^5D_4 \rightarrow {}^7F_5$) is predominant. Taking the PL intensity of 543 nm as a reference, it can be seen from Fig. 7b that with the increase of Tb^{3+} doping concentration, the PL intensities of the phosphors increase firstly and reach the maximal value when the doping concentration of Tb^{3+} is at 10 mol%, then decrease with the continuous increase of Tb^{3+} concentration. Figure 7c shows the corresponding CIE chromaticity coordinate diagram of the phosphors. The CIE chromaticity coordinates of 7, 8, 9, 10, 11, 12 and 13 mol% Tb^{3+}-doped phosphors are (0.2467, 0.5408), (0.2516, 0.5509), (0.2406, 0.5374), (0.256, 0.5607), (0.255, 0.5605), (0.2505, 0.5352), and (0.2566, 0.5374), respectively. The phosphors also display a color-stability property upon the variation of Tb^{3+}-doping concentration, the luminous color of the phosphors is all in the pure green light region, which is very important for the application of the synthesized samples as a green phosphor in the related fields.

The PL properties of $(Lu, Gd)_2O_3$: Ce^{3+}, Tb^{3+} phosphors upon UV excitation are determined by transitions between f-electron and d-electron states of Ce^{3+} and between different f-electron states of Tb^{3+}, which is schematically shown in Fig. 8. Upon UV excitation, electrons of Ce^{3+} in the 4f ground state are populated to the higher 5d excited state, and then relax to the lowest splitting 5d state non-radiatively. Some of the excited electrons come back to $^2F_{7/2}/^2F_{5/2}$ levels and generate 5d-4f emission of Ce^{3+}, other electrons relax non-radiatively to the 4f ground state and transfer the energy to Tb^{3+} by ET process to populate $^5D_3$ and $^5D_4$ levels of Tb^{3+}. Subsequent radiative transitions between the excited $^5D_4$ state and the ^7F_J ($J = 0$–6) ground states of Tb^{3+} generate strong green luminescence, and the emission $^5D_4 \rightarrow {}^7F_5$ centered at 543 nm is predominant [1, 2, 11, 32]. Figure 9a shows the PL spectra of the $(Lu_{0.747}Gd_{0.15}Ce_{0.003}Tb_{0.1})_2O_3$ phosphor sample upon 243 nm, 278 nm and 305 nm excitation. It is noted that the excitation wavelength does not change the location and shape of the emission bands, which means the energy level transitions of the PL emission processes are the same. Meanwhile, excitation wavelength has obvious influence on the PL emission intensity of the phosphor samples, the sample with 243 nm excitation has the strongest PL intensity. Figure 9b shows the corresponding CIE chromaticity coordinate diagram of the sample, the CIE chromaticity coordinates of 243 nm, 278 nm and 305 nm-excited sample are (0.256, 0.5607), (0.2512, 0.5295), and (0.2552, 0.5399), respectively. It can be seen that the change of excitation wavelength can slightly affect the luminous color of the phosphor, which generally shifts from green to green–blue region with the increase of excitation wavelength from 243 to 305 nm.

In addition to being excited by UV light, the as-prepared $(Lu, Gd)_2O_3$: Ce^{3+}, Tb^{3+} phosphors can also be excited by cathode ray. Figure 10a illustrates the CL spectra of the synthesized $(Lu_{0.8-x}Gd_{0.15}Ce_xTb_{0.05})_2O_3$ ($x = 0.1$–0.6 mol%) phosphors upon the excitation of cathode ray (accelerating voltage = 12 kV). Upon the excitation of cathode ray, the $(Lu, Gd)_2O_3$: Ce^{3+}, Tb^{3+} phosphors exhibit a strong green emission, the CL emission bands of the phosphors are similar to that of the PL emission bands, indicating the similarity of the emission mechanism of the two luminescence modes

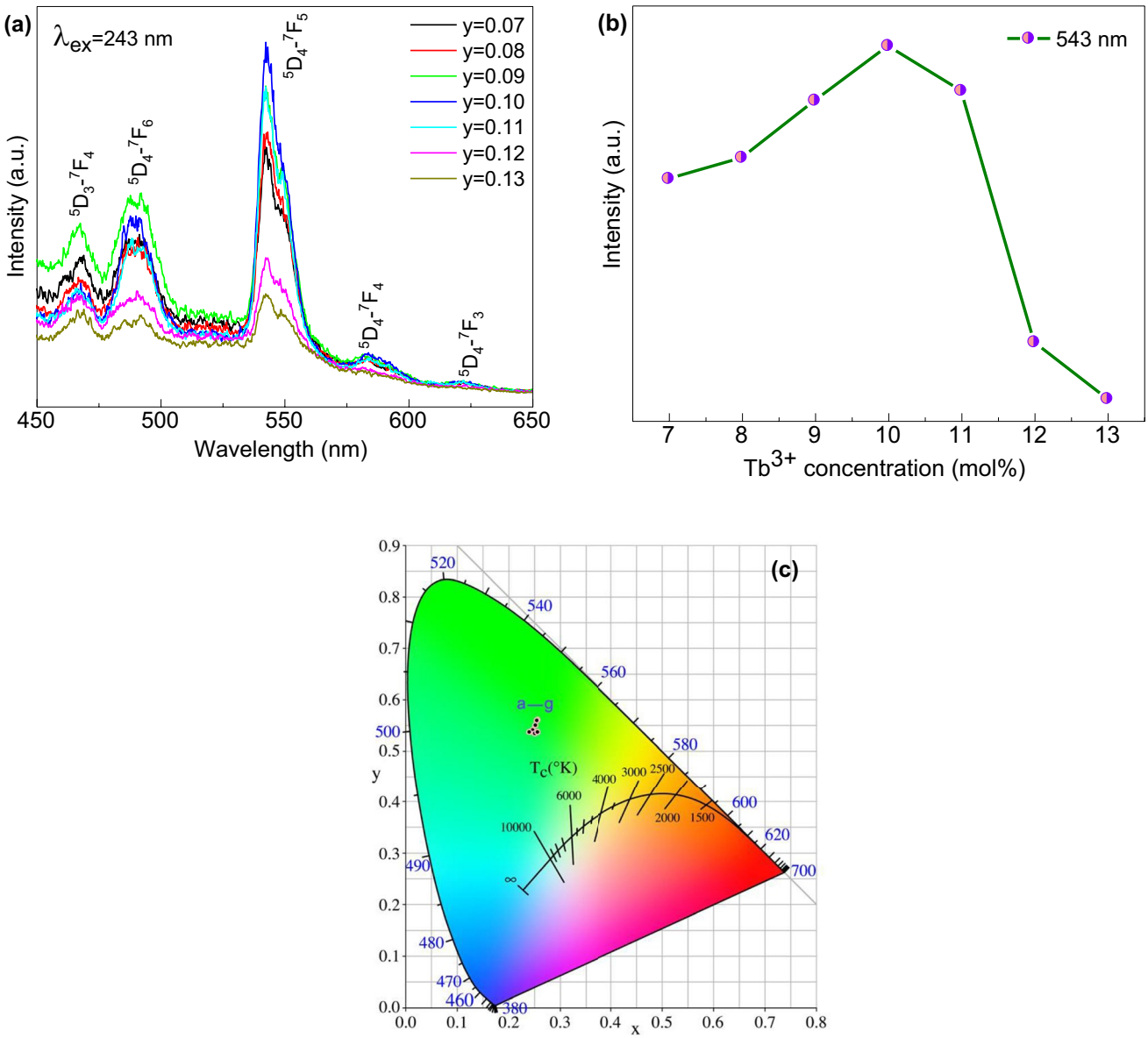

Fig. 7 **a** PL spectra of the $(Lu_{0.847-y}Gd_{0.15}Ce_{0.003}Tb_y)_2O_3$ ($y = 7$–13 mol%) phosphors ($\lambda_{ex} = 243$ nm); **b** PL intensity of Tb^{3+} (543 nm) as a function of Tb^{3+} doping concentration; **c** CIE chromaticity coordinate diagram

[4, 35, 36]. The CL spectra of $(Lu, Gd)_2O_3$: Ce^{3+}, Tb^{3+} phosphors consist of four emission bands, corresponding to the $^5D_4 \rightarrow {}^7F_J$ ($J = 6$, 5, 4, and 3) transitions of Tb^{3+}, respectively, the $^5D_4 \rightarrow {}^7F_5$ transition at 543 nm has the strongest emission intensity. Figure 10b shows the CL intensities of the $(Lu_{0.8-x}Gd_{0.15}Ce_xTb_{0.05})_2O_3$ ($x = 0.1$–0.6 mol%) phosphors at 543 nm as a function of Ce^{3+} doping concentration. The CL intensities of the phosphors increase firstly with the increase of Ce^{3+} concentrations, and reach the maximal value when the Ce^{3+} content is at 0.4 mol%, then decrease with the continuous increase of Ce^{3+} concentration. The corresponding CIE chromaticity coordinate diagram of the phosphors is shown in Fig. 10c, the CIE chromaticity coordinates of 0.1, 0.2, 0.3, 0.4, 0.5 and 0.6 mol% Ce^{3+}-doped phosphors are (0.3654, 0.5465), (0.356, 0.5535), (0.3305, 0.571), (0.3308, 0.571), (0.3299, 0.576), and (0.3704, 0.5425), respectively. It can be seen from Fig. 10c that upon the excitation of cathode ray, the $(Lu, Gd)_2O_3$: Ce^{3+}, Tb^{3+} phosphors demonstrate a color-tunable luminescence property. With the increase of Ce^{3+}-doping concentration, the luminous

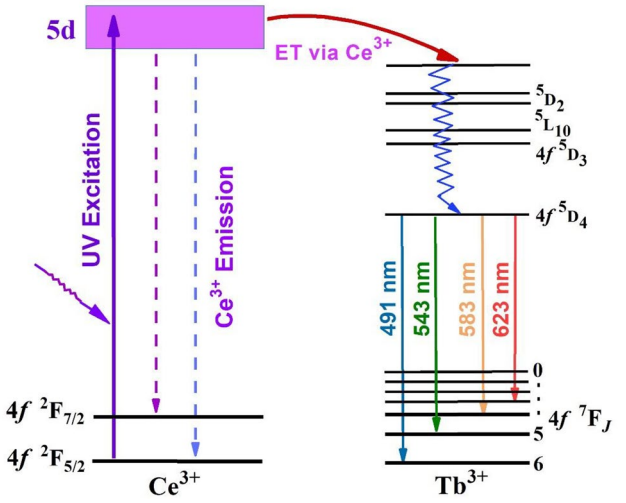

Fig. 8 Schematic diagram of energy transfer between Ce^{3+} and Tb^{3+}

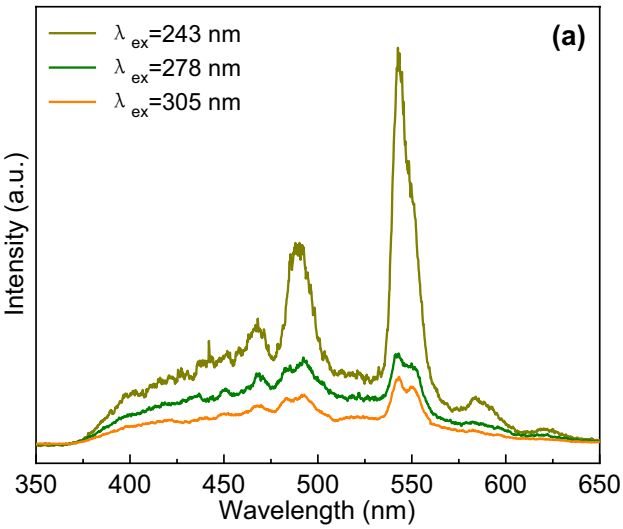

color of the phosphors can be generally adjusted from yellow-green to pure green region, which is different from that of the UV-excited samples. The color-tunable CL property of the (Lu, Gd)$_2O_3$: Ce^{3+}, Tb^{3+} phosphors reveals that the synthesized phosphors may be a promising material for the application in the relevant fields, for example in biological imaging and FED device applications [2, 4, 8].

4 Conclusions

A series of (Lu, Gd)$_2O_3$: Ce^{3+}, Tb^{3+} phosphors were prepared by sol–gel method using citric acid as a chelating agent. The synthesized phosphors are well-crystallized and display a pure Lu_2O_3 phase, indicating the successful formation of (Lu, Gd)$_2O_3$ solid solution host. The SEM analysis indicate that the phosphors show approximately spherical morphology and uniform particle size distribution, and the particle size is at nanoscale. The EDS analysis indicates that the elements of Lu, Gd, Ce and Tb are doped uniformly into the phosphors. Upon the excitation of UV light, the PL spectra of the (Lu, Gd)$_2O_3$: Ce^{3+}, Tb^{3+} phosphors with different Ce^{3+} doping contents consist of four emission peaks centered at 491, 543, 583 and 623 nm, which correspond to the $^5D_4 \rightarrow {}^7F_J$ (J = 6, 5, 4, and 3) transition of Tb^{3+} ions, respectively. The green light emission originating from the $^5D_4 \rightarrow {}^7F_5$ transition (543 nm) has the strongest PL intensity. Taking the PL intensity of $^5D_4 \rightarrow {}^7F_5$ transition as a reference,

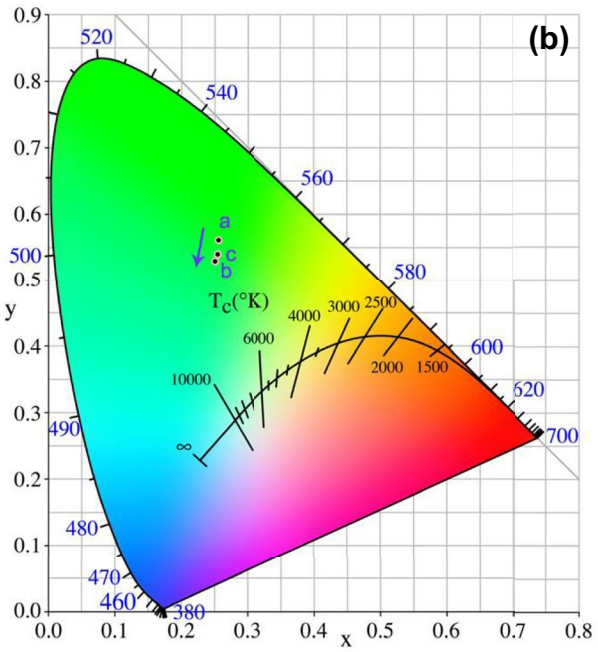

Fig. 9 **a** PL spectra of the ($Lu_{0.747}Gd_{0.15}Ce_{0.003}Tb_{0.1}$)$_2O_3$ phosphor upon excitation of different wavelength; **b** CIE chromaticity coordinate diagram

with the increase of Ce^{3+} concentration, the PL intensities of the phosphors increase firstly and reach the maximal value when the Ce^{3+} content is at 0.3 mol%, then decrease with the continuous increase of Ce^{3+} concentration. The PL spectra of the (Lu, Gd)$_2O_3$: Ce^{3+}, Tb^{3+} phosphors with different Tb^{3+} doping contents consist of five emission peaks, the emission peaks at 468 nm can be assigned to the $^5D_3 \rightarrow {}^7F_4$ transition of Tb^{3+} ion., and

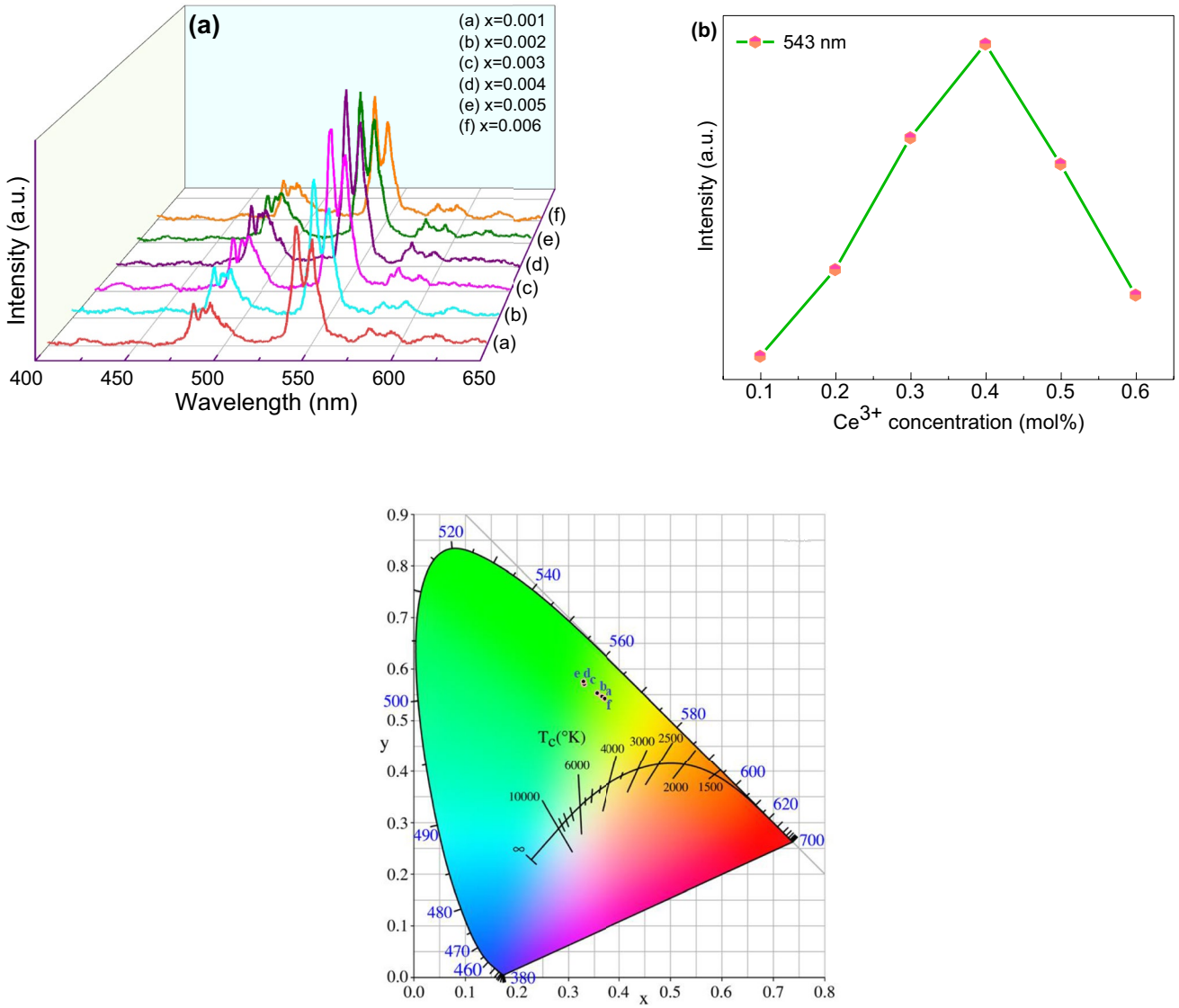

Fig. 10 **a** CL spectra of the $(Lu_{0.8-x}Gd_{0.15}Ce_xTb_{0.05})_2O_3$ ($x = 0.1$–0.6 mol%) phosphors; **b** CL intensity of Tb^{3+} (543 nm) as a function of Ce^{3+} doping concentration; **c** CIE chromaticity coordinate diagram

the peaks at 491, 543, 583 and 623 nm are due to transitions of $^5D_4 \rightarrow {}^7F_J$ ($J = 6$, 5, 4, and 3) transition of Tb^{3+} ions, respectively. Among the five emission peaks, the green emission at 543 nm ($^5D_4 \rightarrow {}^7F_5$) is predominant. With the increase of Tb^{3+} doping concentration, the PL intensities of the samples at 543 nm increase firstly and reach the maximal value when the doping content of Tb^{3+} is at 10 mol%, then decrease with the continuous increase of Tb^{3+} concentration. The $(Lu, Gd)_2O_3$: Ce^{3+}, Tb^{3+} phosphors excited by cathode ray show luminescence spectra similar to that of the samples excited by UV light and a color-tunable luminescence property. The research results of the work indicate that the synthesized $(Lu, Gd)_2O_3$: Ce^{3+}, Tb^{3+} phosphors have potential applications in the fields of three-base color w-LEDs, CL phosphors, FED devices, biological imaging, and so on..

Funding

The authors have not disclosed any funding.

Data availability

Data will be made available on reasonable request.

Declarations

Competing interests The author declare that he have no known competing financial interests or personal relationships that could have appeared to influence the work reported in this paper.

References

1. Y. Zhao, S. Wang, Y. Han, J. Zhang, C. Liu, X. Hu, Z. Zhang, L. Wang, Luminescence properties and energy transfer in Ce^{3+} and Tb^{3+} co-doped $Sr_5(PO_4)_2SiO_4$ phosphor. J. Lumin. **223**, 117253 (2020)
2. Z. Wang, Q. Zhu, X. Wang, X. Li, X. Sun, B. Kim, J. Li, Multi-color luminescent m-$LaPO_4$: Ce/Tb monospheres of high efficiency via topotactic phase transition and elucidation of energy interaction. Inorg. Chem. **58**, 890–899 (2019)
3. E.H. Penilla, Y. Kodera, J.E. Garay, Blue-green emission in terbium-doped alumina (Tb: Al_2O_3) transparent ceramics. Adv. Funct. Mater. **23**, 6036–6043 (2013)
4. D. Fan, S. Yang, J. Wang, A. Zheng, X. Song, D. Yu, Synthesis and cathodoluminescent properties of Y_2SiO_5: Tb^{3+} phosphors prepared from uniform precursor. J. Lumin. **132**, 1122–1125 (2012)
5. M.D. Mehare, C.M. Mehare, H.C. Swart, S.J. Dhoble, Recent development in color tunable phosphors: a review. Prog. Mater. Sci. **133**, 101067 (2023)
6. Y. Huang, T. Li, M. Lei, X. Huang, T. Wang, Efficient one-pot synthesis of bright blue-emitting Ce^{3+}-based phosphor: application for the construction of warm white-light-emitting diodes and anticounterfeiting. ACS Appl. Electron. Mater. **4**, 3575–3582 (2022)
7. Y. Tian, J. Chen, X. Yi, R. Jiang, H. Lin, Y. Tang, S. Zhou, Emission-enhanced high-performance Al_2O_3-Ce: (Y, Tb) AG composite ceramic phosphors for high-brightness white LED/LD illumination. Ceram. Int. **49**, 2698–2704 (2023)
8. T. Furukawa, S. Fukushima, H. Niioka, N. Yamamoto, J. Miyake, T. Araki, M. Hashimoto, Rare-earth-doped nanophosphors for multicolor cathodoluminescence nanobioimaging using scanning transmission electron microscopy. J. Biomed. Optics. **20**, 056007 (2015)
9. E. Pavel, V. Marinescu, M. Lungulescu, B. Sbarcea, Hydrothermal synthesis of β-$NaYF_4$: Ce, Tb crystals doped with different cerium concentrations. Mater. Lett. **210**, 12–15 (2018)
10. X. Fu, L. Fang, S. Niu, H. Zhang, Luminescence properties and energy transfer investigations of $SrMgSi_2O_6$: Ce, Tb phosphors. J. Lumin. **142**, 163–166 (2013)
11. S. Nagashima, K. Ueda, T. Omata, Site-dependent Tb^{3+} luminescence by energy transfer from Ce^{3+} in Ce^{3+}-Tb^{3+} codoped $LaLuO_3$. J. Phys. Chem. C **126**, 6499–6504 (2022)
12. Y. Li, Y. Yin, T. Wang, J. Wu, J. Zhang, S. Yu, M. Zhang, L. Zhao, W. Wang, Ultra-bright green-emitting phosphors with an internal quantum efficiency of over 90% for high-quality WLEDs. Dalton Trans. **50**, 4159–4166 (2021)
13. D. González-Mancebo, A.I. Becerro, T.C. Rojas, A. Olivencia, A. Corral, M. Balcerzyk, E. Cantelar, F. Cussó, M. Ocaña, Room temperature synthesis of water-dispersible Ln^{3+}: CeF_3 (Ln=Nd, Tb) nanoparticles with different morphology as bimodal probes for fluorescence and CT imaging. J. Colloid Interface Sci. **520**, 134–144 (2018)
14. B. Zhao, D. Shen, J. Yang, S. Hu, X. Zhou, J. Tang, Lanthanide-doped Sr_2ScF_7 nanocrystals: controllable hydrothermal synthesis, the growth mechanism and tunable up/down conversion luminescence properties. J. Mater. Chem. C **5**, 3264–3275 (2017)
15. D.R. Cooper, J.A. Capobianco, J. Seuntjens, Radioluminescence studies of colloidal oleate-capped β-Na(Gd, Lu)F_4: Ln^{3+} nanoparticles (Ln=Ce, Eu, Tb). Nanoscale **10**, 7821–7832 (2018)
16. B. Li, J. Liang, L. Sun, S. Wang, Q. Sun, B. Devakumar, G. Annadurai, D. Chen, X. Huang, Y. Wu, Cyan-emitting $Ba_3Y_2B_6O_{15}$: Ce^{3+}, Tb^{3+} phosphor: a potential color converter for near-UV-excited white LEDs. J. Lumin. **211**, 388–393 (2019)
17. Y. Zhang, X. Zhang, H. Zhang, Z. Wu, Y. Liu, L. Ma, X. Wang, W. Liu, B. Lei, Enhanced absorption of $Sr_3Lu_2(BO_3)_4$: Ce^{3+}, Tb^{3+} phosphor with energy transfer for UV-pumped white LEDs. J. Alloys Compd. **789**, 215–220 (2019)
18. A. Oza, V. Ojha, S. Dhale, S. Dhoble, Photoluminescence and thermoluminescence in Dy^{3+}-, Ce^{3+}-, and Tb^{3+}-activated MgB_4O_7 phosphor for dosimetry application. Luminescence **37**, 1563–1574 (2022)
19. W.B. Dai, J. Zhou, K. Huang, J. Hu, S. Xu, M. Xu, Investigation on structure and optical properties of down-conversion aluminosilicate phosphors $CaAl_2Si_2O_8$: Ce/Tb/Yb. J. Alloys Compd. **786**, 662–667 (2019)
20. W. Mi, J. Zheng, P. Qiao, L. Cao, S. Chu, H. Ma, Tunable luminescence, energy transfer and excellent thermal stability of $SrMg_2(PO_4)_2$: Ce^{3+}, Tb^{3+} phosphors for LEDs. J. Rare Earths **39**, 19–25 (2021)

21. P. Liaparinos, C. Michail, I. Valais, G. Fountos, A. Karabotsos, I. Kandarakis, Grain size distribution analysis of different activator doped Gd_2O_2S powder phosphors for use in medical image sensors. Sensors **22**, 8702 (2022)
22. M. Cao, J. Xu, C. Hu, H. Kou, Y. Shi, H. Chen, J. Dai, Y. Pan, J. Li, Fabrication and characterization of (Lu, $Gd_)2_O3$: Eu scintillation ceramics. Ceram. Int. **43**, 2165–2169 (2017)
23. H. Rétot, S. Blahuta, A. Bessière, B. Viana, B. LaCourse, E. Mattmann, Improved scintillation time response in $(Lu_{0.5}Gd_{0.5})_2O_3$: Eu^{3+} compared with Lu_2O_3: Eu^{3+} transparent ceramics. J. Phys. D Appl. Phys. **44**, 235101 (2011)
24. Z. Xu, J. Yang, Z. Hou, C. Li, C. Zhang, S. Huang, J. Lin, Hydrothermal synthesis and luminescent properties of Y_2O_3: Tb^{3+} and Gd_2O_3: Tb^{3+} microrods. Mater. Res. Bull. **44**, 1850–1857 (2009)
25. R.M.K. Whiffen, Ž Antić, A. Speghini, M.G. Brik, B. Bártová, M. Bettinelli, M.D. Dramićanin, Structural and spectroscopic studies of Eu^{3+} doped Lu_2O_3–Gd_2O_3 solid solutions. Opt. Mater. **36**, 1083–1091 (2014)
26. G. Adachi, N. Imanaka, The binary rare earth oxides. Chem. Rev. **98**, 1479–1514 (1998)
27. B. Lu, J. Li, Y. Sakka, Controlled processing of (Gd, $Ln)_2O_3$: Eu (Ln=Y, Lu) red phosphor particles and compositional effects on photoluminescence. Sci. Technol. Adv. Mater. **14**, 064202 (2013)
28. J.I. Langford, A.J.C. Wilson, Scherrer after sixty years: a survey and some new results in the determination of crystallite size. J. Appl. Cryst. **11**, 102 (1978)
29. V. Uvarov, I. Popov, Metrological characterization of X-ray diffraction methods for determination of crystallite size in nano-scale materials. Mater. Charac. **85**, 111 (2013)
30. J. Li, H. Dong, F. Yang, L. Sun, Z. Zhao, R. Bai, H. Zhang, Simple preparation of $LaPO_4$: Ce, Tb phosphors by an ionic-liquid-driven supported liquid membrane system. Int. J. Mol. Sci. **20**, 3424 (2019)
31. J. Zhao, X. Wang, Preparation, structure and luminescent performance of Na_2SiF_6:Re^{3+} (Re^{3+}=Eu^{3+}, Tb^{3+}, Ce^{3+}) powders. Appl. Phys. A **125**, 178 (2019)
32. K. Riwotzki, H. Meyssamy, H. Schnablegger, A. Kornowski, M. Haase, Liquid-phase synthesis of colloids and redispersible powders of strongly luminescing $LaPO_4$: Ce, Tb nanocrystals. Angew. Chem. Int. Ed. **40**, 573–576 (2001)
33. X. Wu, Y. Jiao, O. Hai, Q. Ren, F. Lin, H. Li, Photoluminescence, energy transfer, color tunable properties of $Sr_3La(BO_3)_3$:Ce, Tb phosphors. J. Alloys Compd. **730**, 521–527 (2018)
34. C.H. Seager, D.R. Tallant, Interactions of excited activators in rare earth and transition metal doped phosphors and their role in low energy cathodoluminescence. J. Appl. Phys. **91**, 153–165 (2002)
35. P. Psuja, D. Hreniak, W. Stręk, Cathodoluminescent properties of Tb^{3+}-doped yttria nanocrystallites. J. Rare Earths **27**, 574–578 (2009)
36. G. Alarcón-Flores, M. García-Hipólito, M. Aguilar-Frutis, S. Carmona-Téllez, R. Martinez-Martinez, M.P. Campos-Arias, E. Zaleta-Alejandre, C. Falcony, Synthesis and fabrication of Y_2O_3: Tb^{3+} and Y_2O_3: Eu^{3+} thin films for electroluminescent applications: optical and structural characteristics. Mater. Chem. Phys. **149–150**, 34–42 (2015)